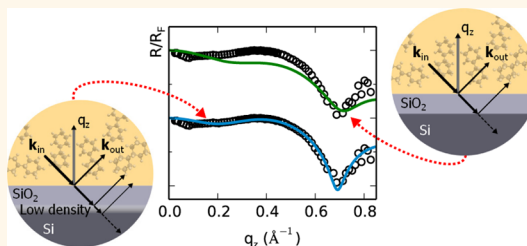# Nanoscale Structure of Si/SiO₂/Organics Interfaces

Hans-Georg Steinrück,[†] Andreas Schiener,[†] Torben Schindler,[†] Johannes Will,[†] Andreas Magerl,[†] Oleg Konovalov,[‡] Giovanni Li Destri,[‡] Oliver H. Seeck,[§] Markus Mezger,[#] Julia Haddad,[∥] Moshe Deutsch,[∥] Antonio Checco,[⊥] and Benjamin M. Ocko*[⊥]

[†]Crystallography and Structural Physics, University of Erlangen-Nürnberg, 91058 Erlangen, Germany, [‡]ESRF, 6 Rue Jules Horowitz, B.P. 220, 38043 Grenoble Cedex, France, [§]HASYLAB am DESY, Notkestrasse 85, 22607 Hamburg, Germany, [#]Max Planck Institute for Polymer Research, Ackermannweg 10, 55128 Mainz, Germany, [∥]Physics Department, and Institute of Nanotechnology and Advanced Materials, Bar-Ilan University, Ramat-Gan 52900, Israel, and [⊥]Condensed Matter Physics & Materials Science Department, Brookhaven National Laboratory, Upton, New York 11973, United States

ABSTRACT X-ray reflectivity measurements of increasingly more complex interfaces involving silicon (001) substrates reveal the existence of a thin low-density layer intruding between the single-crystalline silicon and the amorphous native SiO₂ terminating it. The importance of accounting for this layer in modeling silicon/liquid interfaces and silicon-supported monolayers is demonstrated by comparing fits of the measured reflectivity curves by models including and excluding this layer. The inclusion of this layer, with 6−8 missing electrons per silicon unit cell area, consistent with one missing oxygen atom whose bonds remain hydrogen passivated, is found to be particularly important for an accurate and high-resolution determination of the surface normal density profile from reflectivities spanning extended momentum transfer ranges, now measurable at modern third-generation synchrotron sources.

Polished silicon wafers are by far the most widely used substrates for studying deposited and self-assembled organic thin films due to their low cost and angstrom-scale roughness. Such films are used in organic field-effect transistors,[1−3] photovoltaic devices,[4] biosensors,[5] and more, and for elucidating the basic science underlying self-organization of matter in two dimensions.[6−8] At the surfaces of these wafers the single-crystal silicon is invariably terminated by a few-nanometer-thick native SiO₂ layer, which is, in most cases, amorphous,[9] and the thickness of which is limited by the Cabrera−Mott mechanism.[10] The structure of the transition layer between the silicon and the native oxide is neither well characterized nor well understood at present.[11−13]

A method of choice for studying the structure of Si-wafer-supported organic thin films is X-ray reflectivity (XRR).[14,15] Progress in X-ray beam generation, shaping optics, and detector development at synchrotrons enables extending XRR measurements to larger momentum transfers and lower background scattering. In this article, we show that the combination of (1) different soft-matter terminations of the Si/SiO₂ interface, (2) an extended measurement range, and (3) detailed XRR modeling leads to an improved angstrom-scale resolution description of monolayer organic films and an entirely new representation of the underlying Si/SiO₂ interface.

Tidswell et al.'s pioneering study[16] of the structure of self-assembled monolayers of octadecyltrichlorosilane (OTS) on silicon successfully modeled the SiO₂ layer by a single slab of uniform density, slightly lower than that of silicon. While this model yielded good fits to the XRR measured over the limited momentum transfer range accessible at that time, the resultant Si/SiO₂ interface width was unphysically sharp, only 1 Å. Tidswell's model was subsequently used in numerous studies of silicon-supported organic monolayers[17−26] and for clean thermally grown Si/SiO₂.[27] In these studies an unphysically sharp Si/SiO₂ interface is obtained from the model fits. We note that for many self-assembled monolayers, such as OTS, reliable studies are made possible by the low-energy surface,
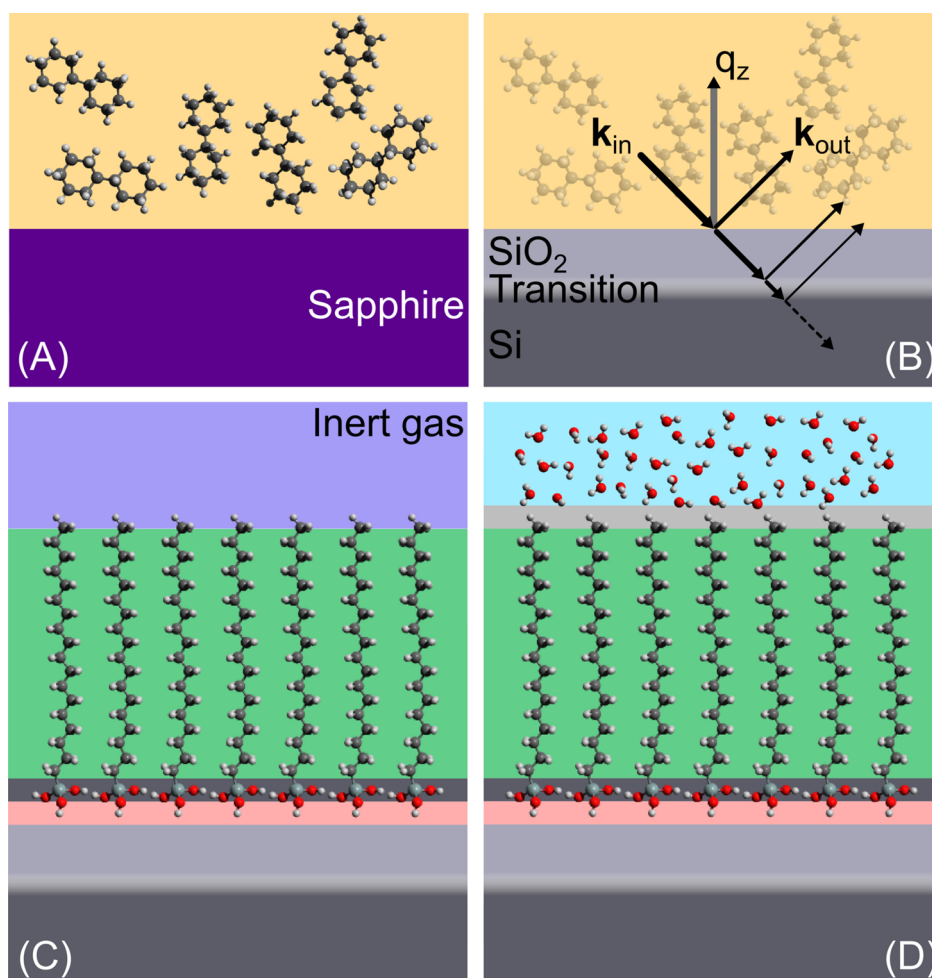
Figure 1. Molecular illustrations of the interfaces studied. XRRs of (a) and (b) are shown in Figure 2, XRR of (c) is shown in Figure 3, and XRR of (d) is shown in Figure 4. The arrows in (b) represent the reflected and refracted beam at each interface.

which prevents the adsorption of contaminants without the need for UHV conditions.

We present here a high-resolution XRR study of native-oxide-terminated (001)-cut silicon substrates (1) in contact with an organic liquid, (2) covered by an OTS monolayer, and (3) covered by an OTS monolayer and in contact with water. A sapphire (0001) substrate in contact with the same organic liquid is also studied, for comparison. Molecular illustrations of these interfaces are presented in Figure 1. The study reveals a hitherto unreported low-density layer at the junction between the truncated silicon lattice and the native oxide. The inclusion of this layer in models for silicon-supported organic monolayers yields for the first time physically acceptable values for all of the model-defining parameters, including those of the oxide.

EXPERIMENTAL SECTION

XRR measures $R(q_z)$, the reflected intensity fraction of an X-ray beam of wavelength λ incident on a sample at a grazing incident angle α. $q_z = (4\pi/\lambda) \sin \alpha$ is the surface-normal scattering vector, shown in Figure 1a. $R(q_z)$ is related, within the first Born approximation,[14,15] to the surface-normal (z) electron density profile $\rho(z)$ through a Fourier transform, $R(q_z) = R_F(q_z)|\rho_0^{-1} \int (d\rho(z)/dz) \exp(iq_z z) \, dz|^2$. $R_F(q_z)$ is the Fresnel reflectivity of an ideally flat and abrupt interface separating bulks of a density difference ρ_0. A widely used method for extracting a structured interface's $\rho(z)$ from a measured XRR is by modeling the interface by a stack of "slabs", each of a uniform, but variable, electron density, ρ_i, thickness, d_i, and interslab Gaussian roughness of width σ_i.[14,15] $R(q_z)$ corresponding to this model ρ, obtained analytically through the equation above,

is then fitted to the measured XRR curve, yielding the values of ρ_i, d_i and σ_i.

As shown in Figure 1b, each interface in the model splits the incident wave into a reflected and a refracted wave. These interfere in the far field, modulating the measured XRR curve. Thus, it is sometimes possible to infer qualitatively from the modulations of the measured XRR the number, thicknesses, and densities of the slabs that need to be included in a model to successfully describe the observed XRR, as we show below.

RESULTS AND DISCUSSION

Figure 2a (symbols) shows a measured Fresnel-normalized XRR (RRF) of a simple, unstructured, sapphire/bicyclohexyl (BCH) solid/liquid interface (symbols, 2.1,

illustrated in Figure 1a). The bulk liquid termination keeps the substrate's surface clean during the XRR measurements without having to resort to UHV conditions. Sapphire, single-crystal Al_2O_3, has no surface oxide layer distinct from the bulk. Therefore, a model consisting of just two semi-infinite slabs,[29] one representing the sapphire and the other the liquid bulk, provides here a good fit to the data (solid line). The monotonic, finite-width transition between the two bulks in the corresponding density profile in
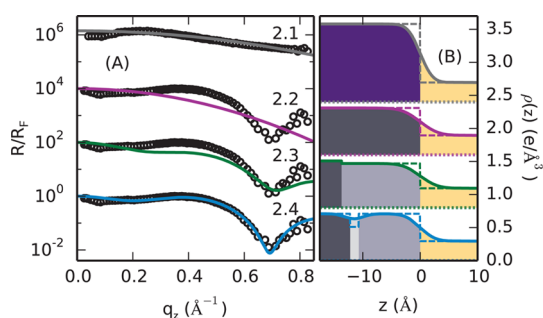

Figure 2. (a) Measured, Fresnel-normalized, X-ray reflectivity (symbols) from a sapphire/bicyclohexyl (BCH) (2.1) and silicon/BCH (2.2−2.4) solid/liquid interface, measured at beamline P08,[28] PETRA III, DESY, with $\lambda = 0.689$ Å. Lines show fits to a simple model of two semi-infinite, uniform-density slabs (2.1 and 2.2, illustrated in Figure 1a) and to a model with a distinct oxide layer, excluding (2.3) and including (2.4, illustrated in Figure 1b) a depletion layer at the SiO_2/silicon interface. (b) Surface-normal density profiles corresponding to the fits in (a) with (solid lines) and without (dashed lines) interfacial roughness. Areal coloring corresponds to Figure 1. All curves are vertically spaced for clarity.

Figure 2b is due to the interfacial roughness. The best-fit parameters, listed in Table 1, are all physically acceptable.

In contrast with the monotonically decreasing RRF of the *sapphire*/BCH interface (symbols, 2.1 in Figure 2a), the *silicon*/BCH interface's RRF (symbols, 2.2−2.4 in Figure 2a) is non-monotonic, exhibiting a pronounced dip at $q_z \approx 0.7$ Å^{-1} and a broad, shallow peak centered at $q_z \approx 0.5$ Å^{-1}. It is not surprising, therefore, that the simple model of two semi-infinite slabs, which reproduced well the former (line, 2.1), is inadequate for the later, as demonstrated in 2.2 (line). Moreover, obtaining a dip in an RRF requires the presence of at least *two* interfaces in order to generate reflected waves that then interfere destructively in the far field due to their different optical path lengths. The presence of such a dip in 2.2 reveals, therefore, the existence of at least one additional interface to the single one observed at the sapphire/BCH model in 2.1. Tidswell's model introduces a second interface by adding between the bulks of the silicon and the BCH an oxide slab of a density slightly lower than that of the silicon. The best fit of this model (line, 2.3 in Figure 2a, and corresponding ρ in Figure 2b) yields an oxide thickness $d_{oxide} = 13.7$ Å. While this model does produce the required dip at $q_z \approx 0.7$ Å^{-1}, in order to yield sufficient depth, the fit drives the Si/SiO_2 interfacial roughness to zero, giving rise to an unphysically sharp interface. Moreover, the shallow peak, mentioned above, and the rise in RRF after the dip are not well reproduced by this model (see 2.3).

TABLE 1. Fit Parameter Values for the Various Samples Shown in Figures 2−4[a]

		sapphire- BCH	Si-BCH			Si-OTS				Si-OTS-(H_2O)[19]	
	curve	2.1	2.2	2.3	2.4	3.1	3.2	3.3	3.4	4.1	4.2
substrate	ρ (e/Å^3)	**1.18**	**0.71**	**0.71**	**0.71**	**0.71**	**0.71**	**0.71**	**0.71**	**0.71**	**0.71**
	σ (Å)	1.7	2.5	0	**1.5**	0	**1.5**	0	**1.5**	**1.5**	**1.5**
Si/SiO$_2$	ρ (e/Å^3)				0.51		0.57		0.56	0.56	0.56
	d (Å)				**1.5**		**1.5**		**1.5**	**1.5**	**1.5**
	σ (Å)				**1.5**		**1.5**		**1.5**	**1.5**	**1.5**
SiO$_2$	ρ (e/Å^3)			0.67	0.71	0.66	**0.71**	0.70	**0.71**	**0.71**	**0.71**
	d (Å)			13.7	10.7	12.4	8.8	15.9	11.3	9.0	9.0
	σ (Å)			2.4	2.1	0.9	2.6	2.6	3.4	3.0	3.0
head group 1	ρ (e/Å^3)					0.54	0.45	**0**	**0**	**0**	**0**
	d (Å)					7.2	8.3	**1.7**	**1.7**	**1.7**	**1.7**
	σ (Å)					4.8	2.5	2.3	2.8	2.6	2.6
head group 2	ρ (e/Å^3)							**0.71**	**0.71**	**0.71**	**0.71**
	d (Å)							**1.7**	**1.7**	**1.7**	**1.7**
	σ (Å)							1.7	3.1	2.5	2.5
alky1 chain	ρ (e/Å^3)					0.29	0.31	0.34	0.31	0.30	0.30
	d (Å)					21.7	19.9	22.4	22.3	21.7	21.7
	σ (Å)					3.2	3.0	2.4	3.0	2.6	2.6
depletion zone	ρ (e/Å^3)										**0**
	d (Å)										1.3
	σ (Å)										2.5
top bulk	ρ (e/Å^3)	**0.33**	**0.33**	**0.33**	**0.33**						**0.33**

[a] Bold values correspond to fixed parameters as discussed in the text.

Following extensive tests with numerous different models, we found that the discrepancy between this model and experiment could be fully eliminated by including an electron depletion layer at the Si/SiO$_2$ interface, as illustrated in Figure 1b. This fit (line, 2.4 in Figure 2a and corresponding ρ in Figure 2b) gives $d_{oxide} = 10.7$ Å, along with a physically acceptable oxide roughness of 2.1 Å. The presence of the depletion layer is also responsible for a more subtle effect. The close-spaced interfaces of this layer give rise to a long-period modulation of the RRF. Over the q_z range measurable here, this modulation provides an increasing-intensity envelope to the amplitude of the shorter-period RRF modulation originating in the two interfaces of the oxide layer. This rising-intensity envelope is responsible for the enhancement of the $q_z \approx 0.5$ Å^{-1} shallow peak and the RRF rise in 2.4 after the dip as compared to 2.3, thus achieving a better fit in 2.4. The measured RRF is now well reproduced by this model over the entire q_z range, thus enhancing the confidence in the corresponding density profile derived (2.4 in Figure 2b).

The inclusion of a depletion layer at the Si/SiO$_2$ interface in the model discussed above is also motivated by experimental studies showing the presence of various oxidation states of silicon at the Si/SiO$_2$ interface,[30−32] in part due to dangling bonds[11] and hydrogen,[9] resulting from the mismatch in bond density between Si and SiO$_2$. Furthermore, theoretical studies also predict an interfacial layer with reduced density,[33] attributed *inter alia* to voids at the Si/SiO$_2$ interface in the Si−O−Si bridge bonds model.[34]

As we have shown in previous studies, for very thin layers,[17,29,35,36] such as the depletion layer at the Si/SiO$_2$ interface, it is not possible to refine d and ρ independently in a fit. The fit is sensitive only to their product. Hence in the fits we used a fixed $d = 1.5$ Å for the transition layer. From this, and the fitted ρ, we calculated that the depletion is equivalent to ~6−8 missing electrons in the electron density profile per unit Si cell area (5.43 Å × 5.43 Å). This corresponds to one missing oxygen atom whose bonds remain hydrogen passivated. The number of missing electrons matches well the value approximated from the model of Morita *et al.*,[9] showing the existence of hydrogen-terminated silicon atoms and voids above the Si−O−Si bridge bonds at the Si/SiO$_2$ interface.[34] The fit-refined oxide thickness, $d_{SiO_2} = 10.7$ Å, also agrees well with literature values for the thickness of the native oxide of silicon determined by X-ray photoelectron spectroscopy.[9]

In the following, we show how the inclusion of the transition oxide region provides for a much improved interpretation of our XRR measurements for OTS self-assembled monolayers prepared on the native SiO$_2$ layer of a silicon substrate, illustrated in Figure 1c. The OTS monolayer was prepared by a well-established procedure[38−40] using a BCH/OTS solution under ambient atmosphere. Whereas other solvents, such
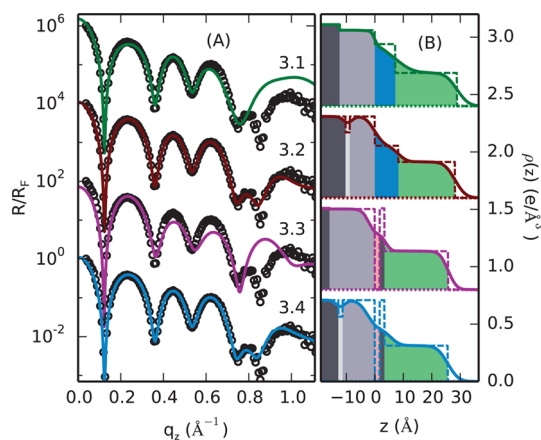

Figure 3. (a) Measured, Fresnel-normalized X-ray reflectivity (symbols) from a silicon-supported OTS monolayer carried out at beamline ID10,[37] ESRF, with $\lambda = 0.590$ Å along with fits (lines) to four different models discussed in the text. (b) Surface-normal electron density profiles corresponding to the respective fits in (a), with (solid lines) and without (dashed lines) surface roughness. Areal coloring conforms to that in Figure 1. The blue corresponds to Tidswell's OTS headgroup model.[16]

as toluene, hexane, and cyclohexane can be successfully used,[41] an ultradry environment[42] provides lower coverage monolayers. In Figure 3, we show our XRR results for the OTS monolayer (symbols) along with fits using four different density profiles (colored lines). In Tidswell's model[16] (line, 3.1 in Figure 3a, and corresponding density profile in Figure 3b), the oxide is described by a lower density slab and the OTS monolayer is described by two slabs, one for the headgroups and one for the alkyl tails. This model provides a poor fit at high q_z. Further, the Si/SiO$_2$ interface is unphyiscally sharp, of width ~0 Å, and the headgroup layer thickness of 7.2 Å is much larger than the expected 3.4 Å Si−O−Si bond length.[43] Inclusion of the depletion layer at the Si/SiO$_2$ interface solves the first two problems and yields an excellent agreement with the measured RRF (3.2), however at the cost of an 8.3 Å headgroup thickness, even thicker and more unphysical than the previous fit (see the corresponding density profile in Figure 3b). As we have shown recently,[44] the larger q_z range now accessible for XRR measurements supports a more detailed and higher-resolution modeling of the OTS headgroups. Here we split the single headgroup's slab into two: a low-density slab adjacent to the native oxide, representing the sparse bonds of the OTS's Si atoms to the native oxide's oxygens, and a high-density one, representing the Si−O−Si cross-links of the OTS molecules. As 3.3 and the corresponding density profile in Figure 3b show, using this more detailed model for the OTS monolayer with the Tidswell model for the Si/SiO$_2$ still provides a poor fit. However, inclusion of the depletion layer at the Si/SiO$_2$ interface (3.4 and corresponding density profile in Figure 3b) yields a near perfect fit over the full, extended q_z range measured, as well as physically acceptable best-fit parameter
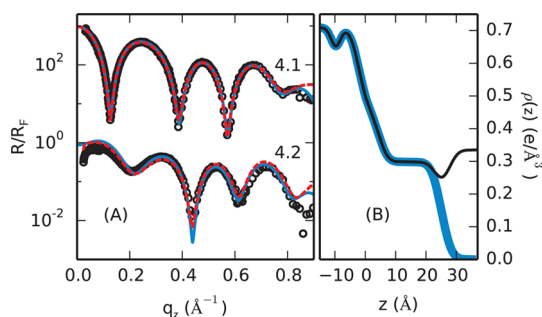
Figure 4. (a) Measured, Fresnel-normalized X-ray reflectivity (symbols), from ref 19, of a dry (4.1) and a water-immersed (4.2) OTS-monolayer-covered silicon substrate, with the original fits from ref 19 (dashed red lines) and the present fits discussed in the text (solid blue lines). (b) Surface-normal electron density profiles corresponding to the present model's fits for the dry (thick blue line) and water-immersed (thin black line) OTS-covered wafers.

values (see Table 1). In particular, the low- and high-density slabs representing the headgroups' layer now have a combined thickness of 3.4 Å. This is in excellent agreement with the Si−O−Si bond length, obtained as twice the 1.7 Å Si−O bond length.[43] Also, the roughness at all interfaces of the slabs describing the OTS monolayer now refines to values within ±0.3 Å of each other, providing a further check on the model's, and fit's, physical acceptability.

To further validate the presence of a depletion slab at the Si/SiO$_2$ interface, we reanalyzed the data of Mezger $et\ al$.[19] employing both the Tidswell model that they used and the present model. These RRF curves, shown in Figure 4a, were measured for dry (4.1) and water-immersed (4.2) OTS-monolayer-covered silicon (001) substrates, prepared similarly to ours, discussed above. For the dry sample our model shows a slight improvement at high q_z over the Tidswell model. For the wet sample, however, the Tidswell and the present model both yield practically overlapping fits (Tidswell's: dashed red line, present: blue line) over the limited q_z range measured. It should be emphasized that identical parameter values were used for fitting both RRF curves, adding only a previously established depletion slab[17,29,35,36] at the OTS/water interface. However, to fit the Si/OTS/water XRR with the Tidswell model, the hydrocarbon layer thickness had to be reduced by ∼7%, as compared to that of the nonimmersed sample.[19] For both models the water density depletion adjacent to the hydrophobic OTS amounts to approximately half a water monolayer. Together, these results further support the validity of our model and, in particular, the presence of a low-density layer at the Si/SiO$_2$ interface.

CONCLUSIONS

In conclusion, using high-resolution XRR measurements on different soft-matter terminations of silicon (001) substrates, we demonstrate the existence of a low-density, few-angstrom-thick, transition layer at the Si/SiO$_2$ interface. This finding supports previous theoretical models and simulations of the Si/SiO$_2$ interface.[34] For the increasingly more complex interfaces measured, we model the surface-normal electron density profiles by both the widely used Tidswell model,[16] which does not include this transition layer, and a new model that includes it. The comparison of the resulting model fits of the measured XRR curves demonstrates that it is imperative to include this layer in the model in order to obtain physically acceptable parameter values, along with a good fit to the measured XRR curve over the full extended q_z range now measurable at third-generation synchrotrons. We hope that this study, resolving discrepancies between measured and model fits of XRRs in specific systems, will enhance the ability to model realistically and accurately other silicon interfaces as well.

REFERENCES AND NOTES

1. Halik, M.; Hirsch, A. The Potential of Molecular Self-Assembled Monolayers in Organic Electronic Devices. *Adv. Mater.* **2011**, *23*, 2689–2695.
2. Schmaltz, T.; Amin, A. Y.; Khassanov, A.; Meyer-Friedrichsen, T.; Steinrück, H. G.; Magerl, A.; Segura, J. J.; Voitchovsky, K.; Stellacci, F.; Halik, M. Low-Voltage Self-Assembled Monolayer Field-Effect Transistors on Flexible Substrates. *Adv. Mater.* **2013**, *25*, 4511–4514.
3. Smits, E. C. P.; Mathijssen, S. G. J.; van Hal, P. A.; Setayesh, S.; Geuns, T. C. T.; Mutsaers, K. A. H. A.; Cantatore, E.; Wondergem, H. J.; Werzer, O.; Resel, R.; *et al*. Bottom-up Organic Integrated Circuits. *Nature* **2008**, *455*, 956–959.
4. Kline, R. J.; Mcgehee, M. D.; Toney, M. F. Highly Oriented Crystals at the Buried Interface in Polythiophene Thin-Film Transistors. *Nat. Mater.* **2006**, *5*, 222–228.
5. Anker, J. N.; Hall, W. P.; Lyandres, O.; Shah, N. C.; Zhao, J.; Van Duyne, R. P. Biosensing with Plasmonic Nanosensors. *Nat. Mater.* **2008**, *7*, 442–453.
6. Onclin, S.; Ravoo, B. J.; Reinhoudt, D. N. Engineering Silicon Oxide Surfaces Using Self-Assembled Monolayers. *Angew. Chem., Int. Ed.* **2005**, *44*, 6282–6304.
7. Schreiber, F. Structure and Growth of Self-Assembling Monolayers. *Prog. Surf. Sci.* **2000**, *65*, 151–256.
8. Ulman, A. Formation and Structure of Self-Assembled Monolayers. *Chem. Rev.* **1996**, *96*, 1533–1554.
9. Morita, M.; Ohmi, T.; Hasegawa, E.; Kawakami, M.; Ohwada, M. Growth of Native Oxide on a Silicon Surface. *J. Appl. Phys.* **1990**, *68*, 1272–1281.
10. Cabrera, N.; Mott, N. F. Theory of the Oxidation of Metals. *Rep. Prog. Phys.* **1949**, *12*, 163.
11. Hattori, T. Chemical Structures of the SiO$_2$/Si Interface. *Crit. Rev. Solid State Mater. Sci.* **1995**, *20*, 339–382.
12. Hirose, K.; Nohira, H.; Azuma, K.; Hattori, T. Photoelectron Spectroscopy Studies of SiO$_2$/Si Interfaces. *Prog. Surf. Sci.* **2007**, *82*, 3–54.
13. Shaikhutdinov, S.; Freund, H.-J. Ultrathin Silica Films on Metals: The Long and Winding Road to Understanding the Atomic Structure. *Adv. Mater.* **2013**, *25*, 49–67.

14. Pershan, P. S.; Schlossman, M. L. *Liquid Surfaces and Interfaces: Synchrotron X-Ray Methods*; Cambridge University Press: Cambridge, UK, 2012.

15. Deutsch, M.; Ocko, B. M. In *Encyclopedia of Applied Physics*; Trigg, G. L., Ed.; VCH: New York, USA, 1998; Vol. 23.

16. Tidswell, I. M.; Ocko, B. M.; Pershan, P. S.; Wasserman, S. R.; Whitesides, G. M.; Axe, J. D. X-Ray Specular Reflection Studies of Silicon Coated by Organic Monolayers (Alkylsiloxanes). *Phys. Rev. B* **1990**, *41*, 1111–1128.

17. Mezger, M.; Reichert, H.; Schöder, S.; Okasinski, J.; Schröder, H.; Dosch, H.; Palms, D.; Ralston, J.; Honkimäki, V. High-Resolution *in Situ* X-Ray Study of the Hydrophobic Gap at the Water/Octadecyl-Trichlorosilane Interface. *Proc. Natl. Acad. Sci. U.S.A.* **2006**, *103*, 18401–18404.

18. Mezger, M.; Sedlmeier, F.; Horinek, D.; Reichert, H.; Pontoni, D.; Dosch, H. On the Origin of the Hydrophobic Water Gap: An X-Ray Reflectivity and MD Simulation Study. *J. Am. Chem. Soc.* **2010**, *132*, 6735–6741.

19. Mezger, M.; Schöder, S.; Reichert, H.; Schröder, H.; Okasinski, J.; Honkimäki, V.; Ralston, J.; Bilgram, J.; Roth, R.; Dosch, H. Water and Ice in Contact with Octadecyl-Trichlorosilane Functionalized Surfaces: A High Resolution X-Ray Reflectivity Study. *J. Chem. Phys.* **2008**, *128*.

20. Richter, A. G.; Yu, C.-J.; Datta, A.; Kmetko, J.; Dutta, P. *In Situ* and Interrupted-Growth Studies of the Self-Assembly of Octadecyltrichlorosilane Monolayers. *Phys. Rev. E* **2000**, *61*, 607–615.

21. Richter, A. G.; Durbin, M. K.; Yu, C.-J.; Dutta, P. *In Situ* Time-Resolved X-ray Reflectivity Study of Self-Assembly from Solution. *Langmuir* **1998**, *14*, 5980–5983.

22. Tidswell, I. M.; Rabedeau, T. A.; Pershan, P. S.; Folkers, J. P.; Baker, M. V.; Whitesides, G. M. Wetting Films on Chemically Modified Surfaces: An X-Ray Study. *Phys. Rev. B* **1991**, *44*, 10869–10879.

23. Wen, K.; Maoz, R.; Cohen, H.; Sagiv, J.; Gibaud, A.; Desert, A.; Ocko, B. M. Postassembly Chemical Modification of a Highly Ordered Organosilane Multilayer: New Insights into the Structure, Bonding, and Dynamics of Self-Assembling Silane Monolayers. *ACS Nano* **2008**, *2*, 579–599.

24. Gutfreund, P.; Wolff, M.; Maccarini, M.; Gerth, S.; Ankner, J. F.; Browning, J.; Halbert, C. E.; Wacklin, H.; Zabel, H. Depletion at Solid/Liquid Interfaces: Flowing Hexadecane on Functionalized Surfaces. *J. Chem. Phys.* **2011**, *134*, 064711.

25. Wolff, M.; Gutfreund, P.; Rühm, A.; Akgun, B.; Zabel, H. Nanoscale Discontinuities at the Boundary of Flowing Liquids: A Look into Structure. *J. Phys.: Condens. Mater.* **2011**, *23*, 184102.

26. Geer, R. E.; Stenger, D. A.; Chen, M. S.; Calvert, J. M.; Shashidhar, R.; Jeong, Y. H.; Pershan, P. S. X-Ray and Ellipsometric Studies of Self-Assembled Monolayers of Fluorinated Chlorosilanes. *Langmuir* **1994**, *10*, 1171–1176.

27. Kosowsky, S. D.; Pershan, P. S.; Krisch, K. S.; Bevk, J.; Green, M. L.; Brasen, D.; Feldman, L. C.; Roy, P. K. Evidence of Annealing Effects on a High-Density SiO_2/Si Interfacial Layer. *Appl. Phys. Lett.* **1997**, *70*, 3119–3121.

28. Seeck, O. H.; Deiter, C.; Pflaum, K.; Bertam, F.; Beerlink, A.; Franz, H.; Horbach, J.; Schulte-Schrepping, H.; Murphy, B. M.; Greve, M.; *et al.* The High-Resolution Diffraction Beamline P08 at PETRA III. *J. Synchrotron Radiat.* **2012**, *19*, 30–38.

29. Ocko, B. M.; Hlaing, H.; Jepsen, P. N.; Kewalramani, S.; Tkachenko, A.; Pontoni, D.; Reichert, H.; Deutsch, M. Unifying Interfacial Self-Assembly and Surface Freezing. *Phys. Rev. Lett.* **2011**, *106*, 137801.

30. Braun, W.; Kuhlenbeck, H. Chemical Structure of Ultrathin Thermally Grown Oxides on a Si (100)-Wafer Using Core Level Photoemission. *Surf. Sci.* **1987**, *180*, 279–288.

31. Himpsel, F. J.; McFeely, F. R.; Taleb-Ibrahimi, A.; Yarmoff, J. A.; Hollinger, G. Microscopic Structure of the SiO_2/Si Interface. *Phys. Rev. B* **1988**, *38*, 6084–6096.

32. Dreiner, S.; Schürmann, M.; Westphal, C. Structural Analysis of the SiO_2/Si(100) Interface by Means of Photoelectron Diffraction. *Phys. Rev. Lett.* **2004**, *93*, 126101.

33. Bongiorno, A.; Pasquarello, A.; Hybertsen, M. S.; Feldman, L. C. Transition Structure at the Si(100)$-SiO_2$ Interface. *Phys. Rev. Lett.* **2003**, *90*, 186101.

34. Tu, Y.; Tersoff, J. Structure and Energetics of the Si-SiO_2 Interface. *Phys. Rev. Lett.* **2000**, *84*, 4393–4396.

35. Ocko, B. M.; Wu, X. Z.; Sirota, E. B.; Sinha, S. K.; Gang, O.; Deutsch, M. Surface Freezing in Chain Molecules: Normal Alkanes. *Phys. Rev. E* **1997**, *55*, 3164–3182.

36. Ocko, B. M.; Dhinojwala, A.; Daillant, J. Comment on "How Water Meets a Hydrophobic Surface". *Phys. Rev. Lett.* **2008**, *101*, 039601.

37. Smilgies, D.-M.; Boudet, N.; Struth, B.; Konovalov, O. Troika II: A Versatile Beamline for the Study of Liquid and Solid Interfaces. *J. Synchrotron Radiat.* **2005**, *12*, 329–339.

38. Maoz, R.; Sagiv, J.; Degenhardt, D.; Möhwald, H.; Quint, P. Hydrogen-Bonded Multilayers of Self-Assembling Silanes: Structure Elucidation by Combined Fourier Transform Infra-Red Spectroscopy and X-Ray Scattering Techniques. *Supramol. Sci.* **1995**, *2*, 9–24.

39. Wen, K.; Maoz, R.; Cohen, H.; Sagiv, J. Postassembly Chemical Modification of a Highly Ordered Organosilane Multilayer: New Insights into the Structure, Bonding, and Dynamics of Self-Assembling Silane. *ACS Nano* **2008**, *2*, 579–599.

40. Pujari, S. P.; Scheres, L.; Marcelis, A. T. M.; Zuilhof, H. Covalent Surface Modification of Oxide Surfaces. *Angew. Chem., Int. Ed.* **2014**, *53*, 6322–6356.

41. Cheng, Y.-a.; Zheng, B.; Chuang, P.-h.; Hsieh, S. Solvent Effects on Molecular Packing and Tribological Properties of Octadecyltrichlorosilane Films on Silicon. *Langmuir* **2010**, *26*, 8256–8261.

42. Peters, R. D.; Nealey, P. F.; Crain, J. N.; Himpsel, F. J. A Near Edge X-Ray Absorption Fine Structure Spectroscopy Investigation of the Structure of Self-Assembled Films of Octadecyltrichlorosilane. *Langmuir* **2002**, *18*, 1250–1256.

43. Weast, R. C. *CRC Handbook of Chemistry and Physics*, 54th ed.; CRC Press: New York, USA, 1974.

44. Steinrück, H.-G.; Magerl, A.; Deutsch, M.; Ocko, B. Pseudorotational Epitaxy of Self-Assembled Octadecyltrichlorosilane Monolayers on Sapphire (0001). *Phys. Rev. Lett.* **2014**, *113*, 156101.